Model predictive control of vehicle charging stations in grid-connected microgrids
An implementation study

Hermans, B.A.L.M.; Walker, S.; Ludlage, J.H.A.; Özkan, L.

DOI
10.1016/j.apenergy.2024.123210

Publication date
2024

Document Version
Final published version

Published in
Applied Energy

Applied Energy 368 (2024) 123210

Contents lists available at ScienceDirect

Applied Energy

journal homepage: www.elsevier.com/locate/apenergy

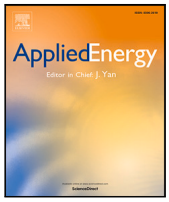

Model predictive control of vehicle charging stations in grid-connected microgrids: An implementation study

B.A.L.M. Hermans [a], S. Walker [b,d], J.H.A. Ludlage [a,e], L. Özkan [a,c,*]

[a] Electrical Engineering Department, Eindhoven University of Technology, Eindhoven, 5612 AP, The Netherlands
[b] Built Environment Department, Eindhoven University of Technology, Eindhoven, 5612 AZ, The Netherlands
[c] Chemical Engineering Department, Delft University of Technology, Delft, 2628 CD, The Netherlands
[d] Kropman B.V., Lagelandseweg 84, Nijmegen, 6545 CG, The Netherlands
[e] CoE MNEXT Avans Hogeschool, Smart Energy Group, Breda, 4818 CR, The Netherlands

ARTICLE INFO

Keywords:
Grid-connected microgrids
Electric vehicle charging
Energy distribution
Model predictive control
Smart grid
Smart charging
Load management
Valley filling
Peak shaving

ABSTRACT

The transition to renewable energy sources, particularly sources like wind and solar induces a dependency on weather in the supply side of electrical grids. At the same time, the move to electric mobility with uncontrolled charging induces extra peak loads on these grids. These developments can cause grid congestion or an imbalance between the renewable power supply and the demand. Locally balancing the power supply and demand in grid-connected microgrids can alleviate such issues on the main grid. This paper presents a model based control strategy to address the challenge of locally balancing the power supply and demand in a grid-connected microgrid to avoid reaching the threshold rated power output set for large buildings. The microgrid under consideration consists of photovoltaic power sources and a large fleet of electric vehicle chargers (> 150). A model predictive controller is developed that treats the daily vehicle charging as a batch process. Given vehicle charge objectives, the controller utilizes vehicle charger occupancy and photovoltaic power generation forecasting services to distribute power optimally over a fixed period of time. The optimization problem is formulated as a quadratic programming problem and is implemented utilizing open-source Python libraries. The controller was integrated into the control system of a microgrid situated at a corporate office in the Netherlands. The control system oversaw the operation of 174 vehicle chargers. The effectiveness of the model predictive control technology was demonstrated over a three-week period and led to an average daily grid peak power reduction of 59%.

1. Introduction

The growing adoption of renewable energy sources such as wind and solar leads to an increasingly decentralized and weather-dependent power supply in electricity grids. The increasing need for electric vehicle charging alters how the electricity grid is utilized. Increasing the share of renewable power while not changing the demand results in a power imbalance over time in the supply and demand [1], a phenomenon apparent in the 'Duck Curve' [2,3]. The Duck Curve is undesirable because it forces grid network operators to rapidly change the power output of conventional power plants to balance the grid. The increase in grid utilization may cause congestion, as seen in some parts of the Dutch electricity grid [4]. Moreover, the recast Energy Performance Building Directive (EPBD) would lower the effective rated output of large buildings from >290 kW to >70 kW [5], making the installation of building automation and control systems mandatory.

Grid-connected microgrids are actors within the electricity grid that can contain local power sources and consumers. Reducing the mismatch between local power demand and supply in microgrids can decrease the likelihood of congestion in the main grid. The goal of this study is to mitigate the local power supply and demand imbalance of an existing operational microgrid by controlling a set of vehicle chargers. Minimizing the imbalance through vehicle charge control results in an optimal control problem.

Solving the optimal control problem in systems that can provide short term flexibility to the power grid and photovoltaic (PV) power sources can be done by optimizing for grid fluctuations [6], operational cost [7], or self-consumption [8]. In such an optimal control problem, if battery energy storage systems (BESSs) are utilized, BESSs are charged when there is surplus PV power and discharged when there is a lack of PV power. Another approach to solving the problem is by implementing vehicle charge control. Optimizing vehicle

* Corresponding author at: Electrical Engineering Department, Eindhoven University of Technology, Eindhoven, 5612 AP, The Netherlands.
E-mail address: l.ozkan@tue.nl (L. Özkan).

https://doi.org/10.1016/j.apenergy.2024.123210
Received 10 January 2024; Received in revised form 17 March 2024; Accepted 8 April 2024
Available online 22 May 2024

Nomenclature

Sets

$\mathbb{R}$, $\mathbb{R}_{\geq 0}$	Real numbers and positive real numbers
$\mathbb{Z}$, $\mathbb{Z}_{\geq 0}$	Integers and positive integers
$\mathbb{K}_{\mathrm{H}}$	Samples in prediction horizon, $\mathbb{K}_{\mathrm{H}} \subset \mathbb{Z}$
$\mathbb{J}_{\mathrm{H}}$	Days in prediction horizon, $\mathbb{J}_{\mathrm{H}} \subset \mathbb{Z}$

Variables

τ	Timestamp [–]
E, ξ, x	Energy [J]
I	Single phase RMS phase current [A]
j	Day index [–]
k	Discrete time index [–]
M	Number of samples or number of days [–]
N	Number of vehicles [–]
P, u, y	Active power [W]
S	Apparent power [VA]
T	Time period [s]
t	Continuous time index [s]
V	Single phase RMS phase voltage [V]

Controller variables

β	Cost function weight parameter [–]
η	Efficiency transmission bus bar [%]
d_1, P_{pv}	Disturbance photovoltaic power [W]
d_2, $N_{\mathrm{connected}}$	Disturbance number of vehicles connected [–]
J	Cost function cost [–]
s	Slack variable optimization problem [W]
u_1	Input power battery energy storage system [W]
u_2	Input power vehicle charging [W]
x_1, E_{b}	Energy state battery energy storage system [J]
x_2, E_{evs}	Energy state vehicle batteries [J]
y, P_{grid}	Output main grid power [W]

Superscripts

$\hat{}$	Measurement
$\tilde{}$	Prediction
$\vec{}$	Three phase current or voltage

Subscripts

0	Start of prediction horizon
j 00:00	Midnight, start of day j
b	Battery energy storage system
charging	Charging number of vehicles
clip	Clipping power
connected	Connected number of vehicles
controlled	Controlled vehicle charge power
daily	Number of vehicles per day
days	Number of days
ev	Single electric vehicle
evs	Aggregated set of electric vehicles
full	Fully charged number of vehicles
grid	Main electricity grid
H	Prediction horizon
max	Maximum
min	Minimum
pv	Photovoltaic
requested	Requested vehicle charge power
s	Sample time or slack variable
T1, T2	Vehicle charge energy objectives 1 and 2

charge control can be done based on the electricity market [9] or by modeling a transportation network in parallel to modeling the electricity network [10]. In literature, model predictive control (MPC) and optimal scheduling algorithms appear to be dominant within such applications. Out of these methods, MPC based applications provide real time adaptability and handle dynamic constraints more effectively. In [11] MPC is used to optimally schedule individual charging sessions in a system containing vehicle chargers, PV power sources, and BESSs. Optimal control solutions to minimize operational cost in systems containing vehicle chargers are presented in [12,13], and [14]. In contrast to the simulation studies [12,13], the solution proposed in [14] is validated on an existing system. Nonetheless, [14] considers vehicle chargers to be an uncontrollable load. Even though research regarding MPC in vehicle charging stations is abundant, according to authors' knowledge no paper presents a successful large-scale implementation of the technology. This might be due to practical challenges such as data availability, system integration or communication and control infrastructure.

This study focuses on a microgrid wherein an MPC based control mechanism is implemented to reduce power peaks induced by EV charging. The study provides valuable insights to literature by demonstrating a fully operational control system in a real-life environment, discussing the lessons learned and results obtained by phenomena such as peak shaving and valley filling while effectively minimizing power imbalance.

The microgrid considered in this study is situated at a large office building in The Netherlands. It consists of controllable vehicle chargers at an aggregated level and a power supply in the form of PV cells. Specifically, the load-balance controller in the infrastructure, which remains unalterable but capable of receiving control inputs, enforces that:

1. The vehicle charge power can only be controlled on an aggregated level rather than controlling individual charging sessions.
2. Power distribution among individual vehicles and load-balancing tasks are delegated to the existing low-level controllers.

A model predictive controller is implemented as the system's optimal inputs depend on uncertain future events. The system is situated near office buildings resulting in periodic behavior of the aggregated vehicle charge power. Therefore, the total vehicle charge energy per day is treated as a single batch of energy due to the periodicity in the charge power. Consequently, the model predictive controller is implemented batch-wise and has a dynamic prediction horizon length. The controller's objective is to minimize the maximum grid power amplitudes while maximizing vehicle charge energy utilizing energy supplied by PV cells. Controller operation depends on vehicle charger occupancy and PV power generation forecasts, which are implemented in a deterministic manner.

The controller is integrated into the existing supervisory control and data acquisition (SCADA) system [15] of the building installation provider. In parallel to the controller development, a vehicle charger occupancy forecast study is performed [16]. The most suitable forecast model developed in [16] is integrated into the controller implementation.

This paper is structured as follows. A dynamic system model of the vehicle charging process and the corresponding controller solution

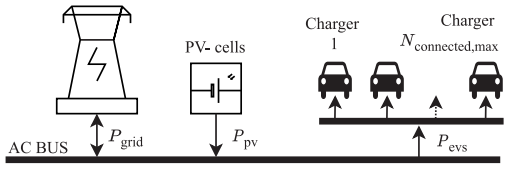

Fig. 1. Simplified power flow diagram from the supervisory controller perspective.

are presented in Section 2 and Section 3, respectively. The controller implementation and integration description is presented in Section 4. The implementation results and conclusions are presented in Section 5 and Section 6, respectively.

2. Dynamic model of the vehicle charging process

The grid-connected microgrid comprises of vehicle chargers and PV cells. A schematic representation of the microgrid is depicted in Fig. 1. Vehicle charge power can only be measured and influenced on an aggregated level since the system does not provide information on individual vehicle chargers. Nonetheless, the total number of charging and fully charged vehicles is available in real time. The dynamic model outlined in this section is utilized to construct an optimal controller that can be applied to any system with a comparable structure. A data analysis on historical charge behavior was conducted prior to modeling the system. Relevant results of the analysis are provided as supplementary material. It was observed that vehicles do not charge during nighttime hours, and that the charging power and charged energy per vehicle both converge to a predictable average when considering charging on an aggregated level.

2.1. System representation

$P_{\text{evs}}(t)$ [W] is the cumulative vehicle charge power and $P_{\text{pv}}(t) > 0$ [W] is solar power. The summation of the elements is the power flowing to or from the main grid $P_{\text{grid}}(t)$ [W] such that;

$$P_{\text{grid}}(t) = P_{\text{evs}}(t) - P_{\text{pv}}(t) \tag{1}$$

The grid power can never exceed the grid power limit $P_{\text{grid,max}}$ such that $-P_{\text{grid,max}} \leq P_{\text{grid}}(t) \leq P_{\text{grid,max}}$.

2.1.1. Vehicle charging

Given the observation that no vehicles charge at night, the vehicle charge energy for one day is considered as a single batch. The cumulative energy provided to the vehicles is $E_{\text{evs}}(t)$ [J]. $E_{\text{evs}}(t)$ follows a first order differential equation. Each day is initiated with 0 such that;

$$E_{\text{evs}}(t) = \int_{00:00}^{t} P_{\text{evs}}(\tau) d\tau \tag{2}$$

$P_{\text{evs}}(t)$ is assumed to be measured at the single interface of the vehicle power distribution bus bar. Every connected vehicle charges within the constraints set by the charging infrastructure. This implies that the actual vehicle charge power depends on either the limit set by the charging infrastructure or on the power requested by the vehicle. $P_{\text{evs,requested}}(t)$ is the cumulative charge power requested by the vehicles if no limits are set by the charging infrastructure. $P_{\text{evs}}(t)$ can be set to a controlled power level $P_{\text{evs,controlled}}(t)$ if $P_{\text{evs,requested}}(t)$ exceeds the clipping threshold $P_{\text{evs,clip}}$, formulated by;

$$P_{\text{evs}}(t) = \begin{cases} P_{\text{evs,requested}}(t) & \text{if } P_{\text{evs,requested}}(t) \leq P_{\text{evs,clip}} \\ P_{\text{evs,controlled}}(t) & \text{if } P_{\text{evs,requested}}(t) > P_{\text{evs,clip}} \end{cases} \tag{3}$$

with $0 \leq P_{\text{evs,clip}} \leq P_{\text{grid,max}}$. This constraint is indirectly imposed by the existing load-balancing controller. Furthermore, $P_{\text{evs,max}}$ is the infrastructure charge limit and $P_{\text{evs,controlled}}(t) \leq P_{\text{evs,max}} \leq P_{\text{grid,max}}$ is enforced at any time. The cumulative requested charge power is dependent on the requested power per vehicle P_{ev} [W] and the number of vehicles charging $N_{\text{charging}}(t) \in \mathbb{Z}_{\geq 0}$ [–]. It is assumed that the charge processes are only controllable by the charge infrastructure if multiple vehicles are charging, $N_{\text{charging}}(t) \gg 0$. Based on the previously mentioned data analysis, on a cumulative level, the charge power per vehicle averages out and is assumed to be constant throughout the charging process. Hence, the power per vehicle P_{ev} is approximated constant and equal for all vehicles, resulting in;

$$P_{\text{evs,requested}}(t) = N_{\text{charging}}(t) P_{\text{ev}} \tag{4}$$

It is assumed that the power is distributed equally among charging vehicles. $N_{\text{connected}}(t) \in \mathbb{Z}_{\geq 0}$ [–] is the number of connected and $N_{\text{full}}(t) \in \mathbb{Z}_{\geq 0}$ [–] is the number of fully charged vehicles, such that;

$$N_{\text{connected}}(t) = N_{\text{charging}}(t) + N_{\text{full}}(t) \tag{5}$$

which is bounded by the number of chargers present in the system $N_{\text{connected,max}}$. Let $j \in \mathbb{Z}$ be an index referring to days. The total number of vehicles connected over the course of day j is $N_{\text{evs,daily}}[j]$ [–].

The system state, input, output, and disturbances are defined by, respectively,

$$x = E_{\text{evs}} \in \mathbb{R} \quad u = P_{\text{evs}} \in \mathbb{R} \quad y = P_{\text{grid}} \in \mathbb{R} \quad d = \begin{bmatrix} P_{\text{pv}} \\ N_{\text{connected}} \end{bmatrix} \in \mathbb{R}^2$$

Following (1) and (2), the system is described by

$$\dot{x}(t) = u(t) \tag{6}$$

$$y(t) = u(t) - d_1(t) \tag{7}$$

where $x(t)$ is set to 0 at midnight. The feasible state space is

$$\mathbb{X} = \{x \in \mathbb{R} \mid x \geq 0\} \tag{8}$$

where an upper bound on the total charge energy x is omitted in this definition as it is dependent on the variable number of vehicles charging. The time-invariant feasible input space is

$$\mathbb{U} = \left\{u \in \mathbb{R} | 0 \leq u \leq P_{\text{evs,max}}\right\} \tag{9}$$

The actual decision space of the controller is a subset of $\mathbb{U}$ since it is dependent on the number of charging vehicles and the control threshold from (3). The feasible output space is

$$\mathbb{Y} = \left\{y \in \mathbb{R} \mid -P_{\text{grid,max}} \leq y \leq P_{\text{grid,max}}\right\} \tag{10}$$

At any time, the disturbances are assumed to be in

$$\mathbb{D} = \left\{ d \in \mathbb{R}^2 \middle| \begin{matrix} 0 \leq d_1 \leq P_{\text{pv,max}}, \\ 0 \leq d_2 \leq N_{\text{connected,max}} \end{matrix} \right\} \tag{11}$$

The system is discretized using the sample time T_s. To ensure that every day is sampled identically, discretization starts at midnight and $\frac{\text{Total time per day}}{T_s} \in \mathbb{Z}$. k is an index referring to discretized time. Assuming zero-order hold for the inputs, the time-invariant model yields;

$$x[k+1] = x[k] + T_s u[k] \tag{12}$$

$$y[k] = u[k] - d_1[k] \tag{13}$$

where $x[k]$ is set to 0 when $t = 00:00$.

3. Controller design for optimal vehicle charging demand

The controller's objective is to maximize vehicle charging utilizing energy supplied by PV cells while minimizing the maximum grid power amplitudes. Maximizing vehicle charging utilizing PV power can be formulated as maximizing self-sufficiency. A batch-type model predictive controller is implemented to solve this problem. It operates in a supervisory fashion as illustrated in the control structure in Fig. 2. The translation from reference power to reference current is performed outside of the model predictive control structure to limit complexity and

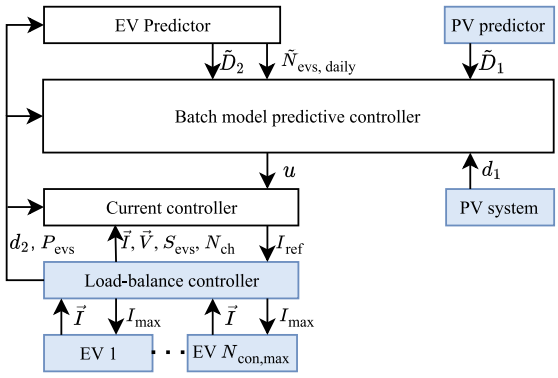

Fig. 2. Supervisory control structure. Items in blue are existing systems. All signals are scalar valued, except $\tilde{D}_1 \in \mathbb{D}^{M_{\text{H}}}$, $\tilde{D}_2 \in \mathbb{D}^{M_{\text{H}}}$, $\vec{I} \in \mathbb{R}^3$ and $\vec{V} \in \mathbb{R}^3$.

to make the controller implementable on a wider variety of systems. Any power converter losses are ignored, and it is assumed that control actions are executed instantaneously.

Each day j, energy targets are set to charge vehicles. The first objective is to deliver a minimal amount of energy $E_{\text{ev,min}}$ to each vehicle by time τ_{T1}. The second objective is to deliver the total requested energy $E_{\text{ev,requested}}$ by time τ_{T2}. The second objective only needs to be achieved if enough PV power is available over the day. The objectives are active every day and are dependent on the total number of vehicles charging per day $N_{\text{evs,daily}}[j]$. Two cumulative energy objectives are established instead of individual vehicle objectives because the system is only controllable on an aggregated level. The two objectives $E_{\text{T1}j}$ and $E_{\text{T2}j}$ refer to the total minimal amount and the total expected amount of energy to be delivered by $\tau_{\text{T1}j}$ and $\tau_{\text{T2}j}$, respectively. Both objectives are defined for all days in the prediction horizon. An optimization problem over a prediction horizon T_{H} [s] is solved on day $j = j_0$ at time $t = t_0$. Sample k_0 corresponds to t_0, and samples $k_{\text{T1}j}$ and $k_{\text{T2}j}$ correspond to $\tau_{\text{T1}j}$ and $\tau_{\text{T1}j}$, respectively. The time-varying sets $\mathbb{J}_{\text{H}} \subset \mathbb{Z}$ and $\mathbb{K}_{\text{H}} \subset \mathbb{Z}$ are the sets referring to the days j and samples k included in the prediction horizon. Suppose a time-invariant T_{H} is considered. In that case, it can occur that for the day j, some samples are included in the horizon, $k \in \mathbb{K}_{\text{H}}$, while the energy objectives are excluded in the horizon, i.e. $k_{\text{T2}j} \notin \mathbb{K}_{\text{H}}$ or $k_{\text{T1}j}, k_{\text{T2}j} \notin \mathbb{K}_{\text{H}}$. Excluding one energy objective in the horizon may result in a sub-optimal result for the day j. Therefore, a batch-type model predictive controller is adopted to ensure consistent inclusion of all energy objectives for all days in the prediction horizon, $k_{\text{T1}j}, k_{\text{T2}j} \in \mathbb{K}_{\text{H}} \forall\, j \in \mathbb{J}_{\text{H}}$. This implies that T_{H} is dynamic and that $t_0 + T_{\text{H}}$ is midnight for any t_0. The static parameter $M_{\text{days}} \in \mathbb{Z}_{>0}$ determines the number of (partial) days included in the prediction horizon. The dynamic number of samples in the prediction horizon is denoted by M_{H}, which is dependent on k_0 and M_{days}. A timeline characterizing the time and naming convention is depicted in Fig. 3(a). During controller operation, the length of the prediction horizon decreases over the day and is extended by one day at the start of a new day, which is depicted in Fig. 3(b).

Optimizing over a prediction horizon requires knowledge of the system's disturbances $d[k] \forall k \in \mathbb{K}_{\text{H}}$ and $N_{\text{evs}}[j] \forall j \in \mathbb{J}$. Disturbance predictions are provided externally and denoted with a $\tilde{}$ and it is assumed that $\tilde{d}[k] \in \mathbb{D}$. Predictions for $\tilde{d}_1[k]$ and $\tilde{d}_2[k] \forall k \in \mathbb{K}_{\text{H}}$ are stacked in the vectors $\tilde{D}_1 \in \mathbb{D}^{M_{\text{H}}}$ and $\tilde{D}_2 \in \mathbb{D}^{M_{\text{H}}}$.

3.1. Control objectives

The control objectives are categorized and included in a cost function. The squared grid power captures both maximizing PV power to charge vehicles and minimizing the grid peak power. Secondly, the deviation from each energy objective in the prediction horizon is included. The third category are slack variable corresponding to the input path constraints, ensuring feasibility.

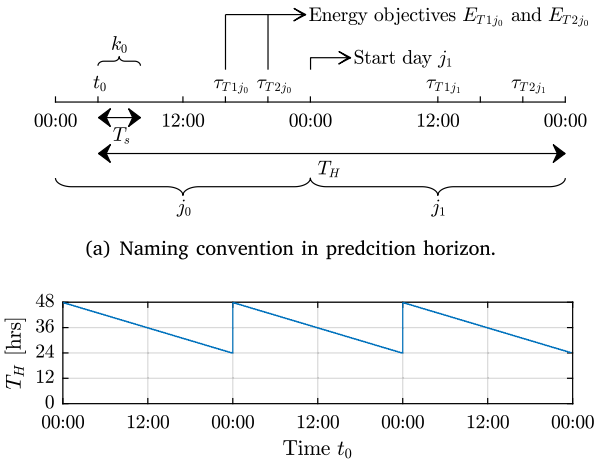

(a) Naming convention in predcition horizon.

(b) Length of prediction horizon T_{H} plotted over time.

Fig. 3. (a) Prediction horizon naming convention and (b) prediction horizon length for $M_{\text{days}} = 2$ such that $\mathbb{J}_{\text{H}} = \{j_0, j_1\}$. The optimization problem is solved at t_0.

3.1.1. Grid power

$y[k] > 0$ implies that grid power is utilized to charge vehicles. $y[k] < 0$ implies that PV power is supplied to the grid and not utilized to charge vehicles. $y[k] = 0$ implies PV power generation and power utilization are in balance, which is the desired condition. The objective to minimize grid power peaks implies that lower power over a more extended period is preferred over high grid power over a shorter period. A cost function with a quadratic structure captures the described objectives

$$\min \sum_{k=k_0}^{k_0+M_{\text{H}}-1} y[k]^2 \tag{14}$$

Given that this cost function is convex solidifies this choice.

3.1.2. Energy objectives

The daily energy targets depend on the total number of vehicles charging daily. The minimal energy to be provided by $\tau_{\text{T1}j}$ and $\tau_{\text{T2}j}$, respectively are

$$E_{\text{T1}j} = \frac{1}{\eta} N_{\text{evs,daily}}[j] E_{\text{ev,min}} \tag{15}$$

$$E_{\text{T2}j} = \frac{1}{\eta} N_{\text{evs,daily}}[j] E_{\text{ev,requested}} \tag{16}$$

$E_{\text{ev,min}}$ is a pre-defined parameter referring the minimum required charge energy per vehicle. $E_{\text{ev,requested}}$ is a pre-defined parameter representing the total expected requested charge energy per vehicle. $E_{\text{ev,min}}$ and $E_{\text{ev,requested}}$ do not take into account any losses that may occur in the internal vehicle's charger. $\eta \in [0, 1]$ is assumed to be time-invariant and incorporates transmission losses that may occur during energy distribution from the bus bar interface down to the individual chargers. Let $\xi_{\text{T1}} \in \mathbb{R}_{\geq 0}^{M_{\text{days}}}$ and $\xi_{\text{T2}} \in \mathbb{R}_{\geq 0}^{M_{\text{days}}}$ be decision variables that refer to the positive deviation from the energy objectives in the prediction horizon. Ideally, those are defined as

$$\xi_{\text{T1}}[j] = \begin{cases} E_{\text{T1}j} - x[k_{\text{T1}j}] & \text{if } x[k_{\text{T1}j}] \leq E_{\text{T1}j} \\ 0 & \text{otherwise} \end{cases} \qquad \forall\, j \in \mathbb{J}_{\text{H}} \tag{17}$$

$$\xi_{\text{T2}}[j] = E_{\text{T2}j} - x[k_{\text{T2}j}] \qquad \forall\, j \in \mathbb{J}_{\text{H}} \tag{18}$$

However, the use of conditional statements is not preferred in a system of equations. As a solution, ξ_{T1} and ξ_{T2} are implemented to act as slack variables in a cost function. The described behavior is captured in the

linear cost function;

$$\min \sum_{j=j_0}^{j_0+M_{\text{days}}-1} \xi_{\text{T1}}[j] + \xi_{\text{T2}}[j] \tag{19}$$

which is constrained by the energy objectives;

$$E_{\text{T1}j} \leq x[k_{\text{T1}j}] + \xi_{\text{T1}}[j] \qquad \forall\, j \in \mathbb{J}_{\text{H}} \tag{19a}$$

$$E_{\text{T2}j} \leq x[k_{\text{T2}j}] + \xi_{\text{T2}}[j] \qquad \forall\, j \in \mathbb{J}_{\text{H}} \tag{19b}$$

$$E_{\text{T2}j} \geq x[k_{\text{T2}j}] \qquad \forall\, j \in \mathbb{J}_{\text{H}} \tag{19c}$$

$$0 \leq \xi_{\text{T1}} \tag{19d}$$

$$0 \leq \xi_{\text{T2}} \tag{19e}$$

where constraint (19c) is added because it is impossible to deliver more energy than requested by the vehicles. A linear cost function is chosen over a quadratic cost function because it offers flexibility in the adjustment of tuning parameters. This allows better differentiation between the different energy objectives.

3.1.3. Priorities

If not enough PV power is available, a trade-off should be made between the individual energy objectives and the grid power usage. The priorities are ordered by;

(a)	Deliver	$E_{\text{T1}j}$ by $\tau_{\text{T1}j}$	$\forall\, j \in \mathbb{J}_{\text{H}}$
(b)	Minimize	$y[k]^2$	$\forall\, k \in \mathbb{K}_{\text{H}}$
(c)	Deliver	$E_{\text{T2}j}$ by $\tau_{\text{T2}j}$	$\forall\, j \in \mathbb{J}_{\text{H}}$

Prioritizing is done by means of weight parameters. Parameter $q_y \in \mathbb{R}_{\geq 0}$ determines the weight per sample $y[k]^2\, \forall\, k \in \mathbb{K}_{\text{H}}$. Parameters $q_{\text{T1}} \in \mathbb{R}_{\geq 0}^{M_{\text{days}}}$ and $q_{\text{T2}} \in \mathbb{R}_{\geq 0}^{M_{\text{days}}}$ determine the weight per energy objective $\forall\, j \in \mathbb{J}_{\text{H}}$. Because of the potentially significant variations in the number of vehicles charging and energy objectives per day, the weight parameter values are dynamic and may change each control iteration. The parameters depend on the disturbance forecast and time. Weight parameter determination and the tuning methodology are described in Section 3.3.3.

3.2. Path constraints

Besides the static constraint $u[k] \in \mathbb{U} \quad \forall\, k$ as stated in (9), extra path constraints are implemented in the optimal control problem, ensuring desired behavior.

3.2.1. Vehicle charging

On top of the energy constraints captured by (19), path constraints on u are implemented determining the charge power limits. The constraints and the resulting decision space are depicted in Fig. 4. The path constraints are determined before solving the optimization problem and are captured by a lower and upper bound;

$$\tilde{u}_{\min}[k] \leq u[k] \leq \tilde{u}_{\max}[k] \quad \forall\, k \in \mathbb{K}_{\text{H}} \tag{20}$$

where both $\tilde{u}_{\min}[k]$ and $\tilde{u}_{\max}[k]$ are dependent on $\tilde{d}[k]$. The upper bound is;

$$\tilde{u}_{\max}[k] = P_{\text{ev}} \tilde{d}_1[k] \quad \forall\, k \tag{21}$$

where it is ignored that vehicles reduce the charge power when approaching or reaching the maximum state of charge (SOC). The lower bound $\tilde{u}_{\min}[k]$ is dependent on the number of vehicles connected $\tilde{d}_2[k]$, the control clipping threshold stated in (3), and the provided charge energy. As Fig. 4. indicates, $\tilde{u}_{\min}[k]$ is approximated to be 0 if the vehicles are theoretically full if charged with $\tilde{u}_{\max}[k]$. This approximation does not capture the system dynamics fully, but is chosen to limit complexity. This exact definition of $\tilde{u}[k]\, \forall\, k \in \mathbb{K}_{\text{H}}$ yields

$$\tilde{u}_{2,\min}[k] = \begin{cases} min(P_{\text{ev}} \tilde{d}_2[k],\ P_{\text{evs,clip}}) & \text{if } x^*[k] < E_{\text{T2}j} \\ 0 & \text{otherwise} \end{cases} \tag{22}$$

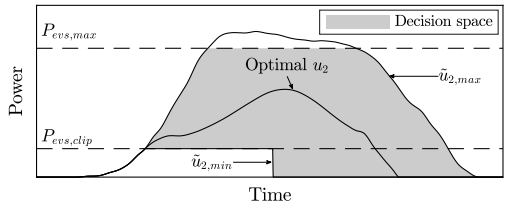

Fig. 4. Decision space u for a single day in the prediction horizon. Constraints related to energy are excluded in the figure.

where $x^*[k]$ is a hypothetical charge energy state if the vehicles are charged with $\tilde{u}_{\max}[k]$. The lower bound ignores scenarios where the vehicles are not fully charged and still request some power by the end of the day.

3.2.2. Soft constraints

The combination of the path constraints in (20) and the energy objectives in (19) may be incompatible and result in an unfeasible optimization problem. Soft constraints are implemented using the slack variables listed in vector $s \in \mathbb{R}_{\geq 0}^{M_{\text{H}}}$. q_s determines the weight for the slack variables in the cost function.

3.3. Optimization problem

The cost minimization objectives are combined into a single cost function $J(u, \xi, s)$. Combining the cost function and corresponding constraints yields the optimization problem;

$$\min_{u,\xi_{\text{T1}},\xi_{\text{T2}},s} \sum_{k=k_0}^{k_0+M_{\text{H}}-1} q_y y[k]^2 + q_s s[k] + \sum_{j=j_0}^{j_0+M_{\text{days}}-1} q_{\text{T1}j} \xi_{\text{T1}}[j] + q_{\text{T2}j} \xi_{\text{T2}}[j] \tag{23}$$

subject to

$$y[k] = u[k] - \tilde{d}_1[k] \qquad \forall k \in \mathbb{K}_{\text{H}} \tag{23a}$$

$$x[k+1] = x[k] + T_{\text{s}} u[k] \qquad \forall k \in \mathbb{K}_{\text{H}} \tag{23b}$$

$$y[k] \in \mathbb{Y} \qquad \forall k \in \mathbb{K}_{\text{H}} \tag{23c}$$

$$x[k] \in \mathbb{X} \qquad \forall k \in \mathbb{K}_{\text{H}} \tag{23d}$$

$$u[k] \in \mathbb{U} \qquad \forall k \in \mathbb{K}_{\text{H}} \tag{23e}$$

$$u[k] \leq \tilde{d}_1[k] \qquad \forall k \in \mathbb{K}_{\text{H}} \tag{23f}$$

$$u[k] \leq \tilde{u}_{\max}[k] + s[k] \qquad \forall k \in \mathbb{K}_{\text{H}} \tag{23g}$$

$$-u[k] \leq -\tilde{u}_{\min}[k] + s[k] \qquad \forall k \in \mathbb{K}_{\text{H}} \tag{23h}$$

$$E_{\text{T1}j} \leq x[k_{\text{T1}j}] - x[k_{j,00:00}] + \xi_{\text{T1}}[j] \qquad \forall j \in \mathbb{J}_{\text{H}} \tag{23i}$$

$$E_{\text{T2}j} \leq x[k_{\text{T2}j}] - x[k_{j,00:00}] + \xi_{\text{T2}}[j] \qquad \forall j \in \mathbb{J}_{\text{H}} \tag{23j}$$

$$-E_{\text{T2}j} \leq -x[k_{\text{T2}j}] + x[k_{j,00:00}] \qquad \forall j \in \mathbb{J}_{\text{H}} \tag{23k}$$

$$0 \leq \xi_{\text{T1}}[j] \qquad \forall j \in \mathbb{J}_{\text{H}} \tag{23l}$$

$$0 \leq \xi_{\text{T2}}[j] \qquad \forall j \in \mathbb{J}_{\text{H}} \tag{23m}$$

$$0 \leq s[k] \qquad \forall k \in \mathbb{K}_{\text{H}} \tag{23n}$$

where $x[k_{j,00:00}]$ in (23i) and (23j) is setting the charge energy state to zero at midnight. It can either be a past measurement, if $j = j_0$, or a function of $u[k]$, if $j > j_0$.

3.3.1. Convexity

Optimization problem (23) is classified as a quadratic program with positive coefficients and linear constraints, indicating convexity.

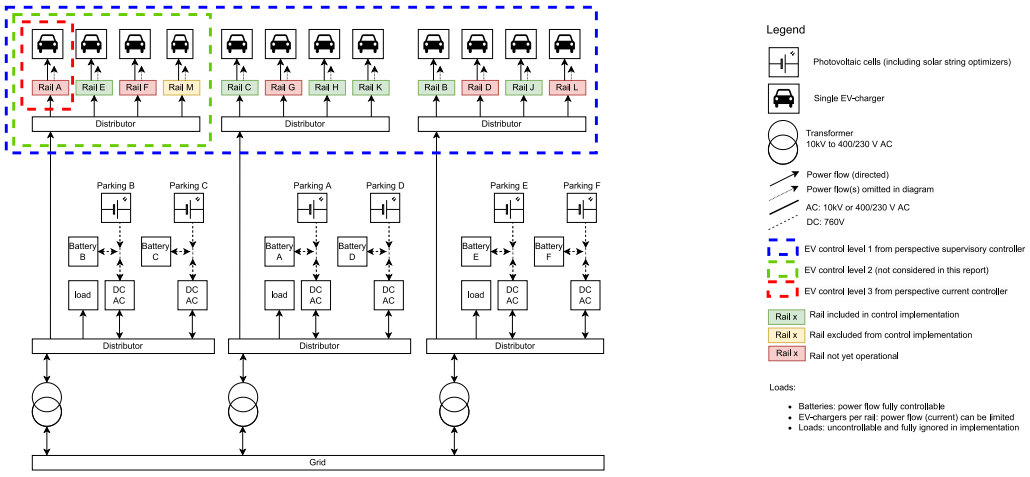

Fig. 5. Simplified schematic representation of the energy distribution system.

Also, $\xi \geq 0$, and $s \geq 0$, and $\mathbb{U}$ is a closed set, confirming that the optimization problem is bounded. The convexity and boundedness of the optimization problem enable the identification of global optima, ensuring consistent controller operation.

3.3.2. Feasibility

It is assumed that the initial measurements and PV power predictions are feasible: $x[k_0] \in \mathbb{X}$, $x[k_0] \leq E_{\mathrm{T2}j_0}$, and $\tilde{d}[k] \in \mathbb{D}\,\forall\, k \in \mathbb{K}_{\mathrm{H}}$. If the soft path constraints, (23g) and (23h), and the minimal energy constraints, (23i), (23j), are ignored, then it is evident that $u[k] = 0$ and $s[k] = 0$, $\forall\, k \in \mathbb{K}_{\mathrm{H}}$, and $\xi_{\mathrm{T1}} = 0$ and $\xi_{\mathrm{T2}} = 0\ \forall j \in \mathbb{J}_{\mathrm{H}}$ is a feasible solution in any situation. The slack variables in s ensure feasibility for (23g) and (23h). The energy target deviations in ξ_{T1} and ξ_{T2} ensure feasibility for (23i) and (23j), respectively.

3.3.3. Tuning

The dynamic cost function weights in q_y, q_{T1}, q_{T2}, and q_s are determined by following a systematic approach first, followed by a trial and error approach. The systematic approach is based on "Bryson's rule" [17, Chapter 9.5]. During the trial and error stage, the parameters are chosen considering the priorities in Section 3.1.3. The parameter $J_{\max}$ defines the maximum cost of $J(u, \xi, s)$ if all variables are at their maximum. The cost function weights are defined as functions of $J_{\max}$, the horizon length M_{H}, and the theoretical maximum of the corresponding variable. The tuning parameter $\beta_y \in \mathbb{R}_{\geq 0}$ sets the relative importance of the squared output, the tuning parameters $\beta_{\mathrm{T1}} \in \mathbb{R}_{\geq 0}$ and $\beta_{\mathrm{T2}} \in \mathbb{R}_{\geq 0}$ set the relative importance of the energy objectives, and the tuning parameter $\beta_s \in \mathbb{R}_{\geq 0}$ sets the relative importance of the slack variables. Let β_Σ be the sum of all β-tuning parameters. With a slight abuse of notation, the dynamic weights are described by

$$q_y = \frac{\beta_y J_{\max}}{\beta_\Sigma M_{\mathrm{H}} y_{\max^2}} \qquad q_s = \frac{\beta_s J_{\max}}{\beta_\Sigma M_{\mathrm{H}} P_{\mathrm{evs,max}}}$$

$$q_{\mathrm{T1}}[j] = \frac{\beta_{\mathrm{T1}} J_{\max}}{\beta_\Sigma E_{\mathrm{T1}j}} \qquad q_{\mathrm{T2}}[j] = \frac{\beta_{\mathrm{T2}} J_{\max}}{\beta_\Sigma E_{\mathrm{T2}j}}$$

4. Implementation

4.1. System and actuation

The grid-connected microgrid powers 174 vehicle chargers and is connected to the medium-voltage electricity grid. A detailed schematic system representation is depicted in Fig. 5.

Vehicle chargers are connected to low-voltage distribution networks via seven AC three-phase rail lines. The rail lines are connected to three separate low-voltage AC distributors. Three 760 V DC grids consisting of PV cells and batteries are connected to the low-voltage distribution systems via bi-directional converters. The low-voltage AC distributors are connected to medium to low-voltage transformers. Transformer, converter, and other component losses are considered negligible.

The control system implementation oversees the operation of six rails, whereas the seventh rail is excluded to accommodate vehicles that might not be compatible with the new control system. The seventh rail is ignored in the results. The six separate rails are each under the control of a distinct load-balance controller, all of which are capable of accepting one control input.

The PV power forecast is provided in real time by the service Solargis [18]. Vehicle charging forecasts are performed in terms of the number of vehicles connected, since this signal is independent of any control signals. The load balance systems' dynamics (see Fig. 2) depend on the number of vehicles connected per rail, the number of phases each vehicle utilizes, and the requested currents. The load balance controller operates in a rule-based manner, and its behavior is out of scope for this study.

4.2. Integration into SCADA system

Python is chosen to implement the control blocks shown in Fig. 2. The state diagram depicted in Fig. 6 describes the behavior of the implemented software and communication with hardware components. A graphical user interface is designed to interact with the system and to view historical, real-time, and predicted system behavior. A screenshot is depicted in Fig. 7. The developed control structure is integrated into the SCADA system of the building named InsiteSuite [15]. The Python controller implementation communicates to InsiteSuite using remote procedure and HTML calls. InsiteSuite communicates with the relevant data acquisition, forecasting and control systems.

4.3. Controller system elements

4.3.1. Model predictive controller

Optimization problem (23) is implemented as a quadratic program, which is solved using the Python library CVXOPT [19].

4.3.2. Heuristic control for current distribution

The reference charge power u_2 is distributed equally among the charging vehicles connected to the six rails. The calculation block 'Current controller' in Fig. 2 is implemented in Algorithm 1. The algorithm allocates the reference charge power u_2 over the six rails by setting the maximum allowable current per rail.

For simplicity of notation, $\mathbf{P}, \mathbf{N}$ and P, N are used to denote the charge power and number of charging vehicles, cumulatively and per

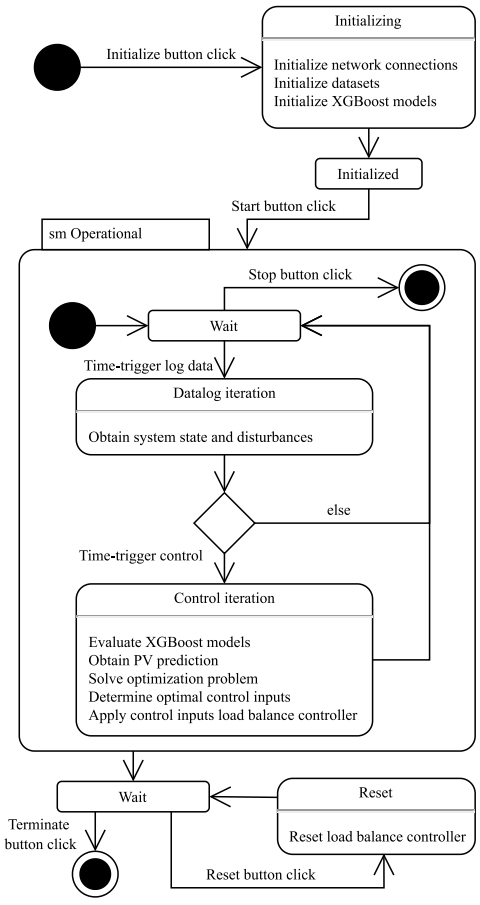

Fig. 6. Simplified state diagram controller implementation.

rail, respectively. For each rail, the reference input current I_{ref} is determined utilizing the measurements for three-phase currents $\vec{I} \in \mathbb{R}^3$, three-phase voltages $\vec{V} \in \mathbb{R}^3$, apparent S [VA] and active power P [W]. A current-delta between the three phases, denoted by $\Delta\vec{I}$, may be present because some vehicles exclusively use one or two phases to charge. The reference input currents are applied without using error feedback because the bandwidth of the load balance controller is equal to the sampling time of the supervisory controller.

Algorithm 1 Current controller

Initialize $\mathbf{P} = u_2$, $\mathbf{N} = \hat{N}_{\text{charging,total}}$
for all Rails **do**
  Obtain N, P, S, $\vec{I}$, $\vec{V}$ ▷ measurements
  $PF = \frac{P}{S}$ ▷ power factor
  $\Delta\vec{I} = max(\vec{I}) - \vec{I}$ ▷ mismatch in phase-currents
  $\vec{I}_{\text{ref,min}} = min(32, \vec{I})$ ▷ minimal current
  $P_{\text{ref,min}} = PF\vec{V}^{\top}\vec{I}_{\text{ref,min}}$ ▷ minimal power
  $P_{\text{ref,optimal}} = \mathbf{P}\frac{N}{\mathbf{N}}$ ▷ optimal power
  if $P_{\text{ref,optimal}} < P_{\text{ref,min}}$ **then** ▷ control impossible
    $\mathbf{P} = \mathbf{P} - P_{\text{ref,min}}$
    $\mathbf{N} = \mathbf{N} - N$
    $I_{\text{ref}} = 32$ A ▷ Minimal I_{ref} yielding $P = P_{\text{ref,min}}$
  end if
end for
for all Rails **do**
  if $P_{\text{ref,optimal}} \geq P_{\text{ref,min}}$ **then** ▷ control possible

$$I_{\text{ref}} = \mathbf{P} \underbrace{\frac{N}{\mathbf{N}}}_{\substack{\text{fraction}\\ \text{total}\\ \text{power}}} \underbrace{\frac{1}{PF}}_{\substack{\text{power}\\ \text{factor}}} \underbrace{\frac{1}{\sum_{i=1}^{3}\vec{V}[i]}}_{\substack{\text{current}\\ \text{per phase}}} + \underbrace{\frac{\vec{V}^{\top}\Delta\vec{I}}{\sum_{i=1}^{3}\vec{V}[i]}}_{\substack{\text{phase}\\ \text{mismatch}\\ \text{compensation}}}$$

  end if
end for

4.3.3. Forecast vehicle occupancy

During the data analysis on historical charge behavior, it was identified that the aggregated vehicle occupancy during the week follows a periodic behavior. This behavior creates an opportunity to predict vehicle charger occupancy using a data-driven approach. A heuristic study that was conducted and published in [20–22] compared the accuracy of different machine learning algorithms in vehicle charger occupancy prediction and concluded that gradient boosting decision tree algorithm (XGBoost) has better performances. However, XGBoost does not predict well beyond the range in the training data [23], which can be taken as a limitation but also can be useful to test the robustness of the model predictive controller of this study. Vehicle charger occupancy is forecasted using the XGBoost algorithm [24]. Given seven consecutive days of historical vehicle occupancy data, the prediction model should return two days of predictions following:

$$f_{\text{XGBoost}} : \mathbb{D}_2^{7M_j} \rightarrow \mathbb{D}_2^{2M_j}$$
$$\hat{d}_2[k_0 - M_{7\ \text{days}} : k_0] \mapsto \tilde{d}_2[k_0 + 1 : k_0 + M_{2\ \text{days}}]$$

To extend the XGBoost model from a single-step prediction into a multi-step structure, multiple models were used to forecast a time series as shown in Fig. 8. For this prediction, the historical number of vehicles $\{15, 30, 45, 60, 75, 90\}$ minutes before, historical number of vehicles $\{1, 2, 3, 4, 5, 6\}$ days before, month, weekday, hour of the day, holiday (boolean) were chosen as model features after performing a feature importance analysis. Using a sample time of 15 min and a prediction horizon of two days, the model training time (85 s) and evaluation time (3 s) are considered adequate for the purpose of this application.

4.4. Auxiliary systems

Auxiliary systems and checks are implemented to increase robustness. These include faulty measurement checks, division by zero checks, a minimal power factor check, and a system ensuring that all measurements and control inputs are withing realistic limits. In the event of a server communication error for any of the data-connections, the controller will still function using the latest obtained data.

4.4.1. Faulty vehicle forecast detection and compensation

The probability of encountering input data that the XGBoost models are not trained for increases with a larger fleet of vehicles or with a change in the number of chargers. Hence, there is a theoretical possibility that the XGBoost models produce forecasts that are unrealistic. Through the use of an independent validation set, the one-step-ahead error metrics for forecasts that are subjectively confirmed to be realistic are determined. The analysis is provided as supplementary material and its results are used as a baseline. Algorithm 2 is used to detect and compensate for faulty predictions. A forecast is considered faulty if the one-step-ahead prediction errors $e[k] \in \mathbb{R}$ exceed the baseline threshold. The decision to use the absolute error rather than a percentage error is based on the possibility of a percentage error becoming disproportionately large in cases where the arrival or departure times are predicted incorrectly.

4.4.2. Vehicle forecast adjustment for fully charged vehicles

The actual vehicle charge limit depends on the N_{charging} instead of $N_{\text{connected}}$. Therefore, for the samples belonging to j_0, the forecast $\tilde{d}_2[k]$ is adjusted for the measured number of fully charged vehicles $\hat{N}_{\text{full}}[k_0]$. It is assumed that fully charged vehicles leave first.

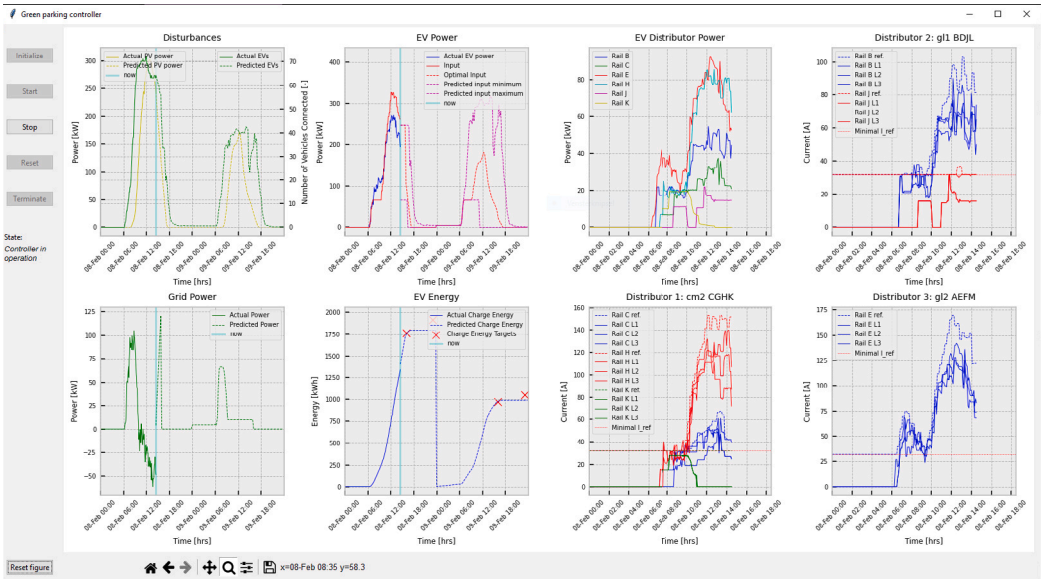

Fig. 7. Screenshot graphical user interface.

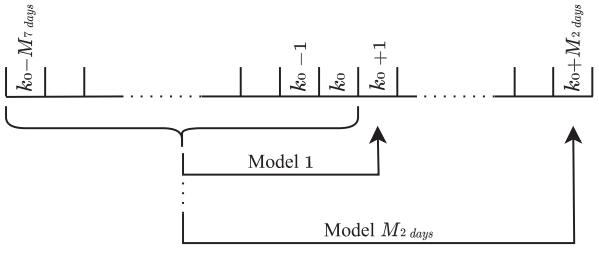

Fig. 8. Multi-step forecast.

Algorithm 3 Energy objective adjustments

if $\hat{x}[k_0] < E_{\mathrm{T1}j_0} \wedge k_0 \geq k_{\mathrm{T1}}$ **then** ▷ Objective not met
  $k_{\mathrm{T1}} = k_0 + 1$ ▷ Push objective forward
end if
$\alpha \in [0, 1]$ ▷ Parameter: % of vehicles stopped charging
if $\alpha \hat{N}_{\mathrm{evs,\ daily}}[j_0] > \hat{N}_{\mathrm{ch}}[k_0]$ **then** ▷ Lower objective if α % stopped
  $E_{\mathrm{T1}j_0} = min(E_{\mathrm{T1}j_0}, \hat{x}_2[k_0] + \hat{N}_{\mathrm{ch}}[k_0] E_{\mathrm{ev,min}})$
end if
$E_{\mathrm{T2}j_0} = max(E_{\mathrm{T2}j_0}, \hat{x}[k_0])$ ▷ Change if charged more than expected

4.4.3. Energy objective adjustments

Algorithm 3 is implemented to cope with situations where energy objectives must be adjusted. The algorithm adds past energy targets to future timestamps if that target is not yet met. It adjusts the energy target downwards if the total charge energy left is out of proportion with the number of vehicles still charging. Lastly, the energy target is adjusted upwards if the total charged energy exceeds the anticipated value.

Algorithm 2 Faulty vehicle forecast detection and compensation

for $k_0 - 3 : k_0$ **do** ▷ determine prediction error
  $e[k] = d_2[k] - \tilde{d}_2[k_{|k-1}]$
end for
if $\begin{cases} |e[k_0]| & > e_{\mathrm{max1}} \vee \\ min(|e[k_0 - 1 : k_0]|) & > e_{\mathrm{max2}} \vee \\ min(|e[k_0 - 2 : k_0]|) & > e_{\mathrm{max3}} \vee \\ min(|e[k_0 - 3 : k_0]|) & > e_{\mathrm{max4}} \vee \end{cases}$ **then** ▷ error detection
  for all $k \in \mathbb{K}_{\mathrm{H}}$ **do** ▷ compensate for faulty prediction
    $\tilde{d}_2[k] = \tilde{d}_2[k] + \frac{M_{\mathrm{H}} + k_0 - k}{M_{\mathrm{H}}} e[k_0]$
  end for
end if

5. Results and discussion

The controller was operational for three weeks in February 2023. An overview of the implementation parameters can be found in Section 5.1. The results are presented and compared to situations where the controller was not operational. Some practical implementation problems are summarized in Section 5.4 and controller limitations are identified in Section 5.5. Performance indicators such as daily grid peak power and self sufficiency are utilized to demonstrate the before and after performance of the implementation.

5.1. Parameters

The implementation parameters and setpoints are listed in Table 1.

Prior to implementation, simulation studies were conducted and concluded that $M_{\mathrm{days}} > 1$ resulted in better performance than a $M_{\mathrm{days}} = 1$. With more than one day in the horizon, the controller could anticipate the following day's energy objectives and PV power supply. Including more than two days in the horizon increased calculation times while not significantly improving the results, so $M_{\mathrm{days}} = 2$ was chosen in the implementation. The cost function tuning parameters were selected following the strategy described in Section 3.3.3.

The efficiency term η in Table 1c is based on historical charge detail records of individual vehicle chargers. This data is compared to the integrated power measurements P_{evs} utilized by the controller. The term does not consider internal vehicle charging losses. $P_{\mathrm{ev,requested}}$ and $E_{\mathrm{ev,requested}}$ were initially chosen to be the arithmetic mean of the charge detail records. However, initial implementation tests concluded that overestimating the terms by respectively 0.31 kW and 0.83 kWh yielded better overall performance. $E_{\mathrm{ev,min}}$ was initially chosen to satisfy the theoretical criterion of enabling each vehicle to cover a round-trip commute distance. Its refinement was carried out iteratively through collaboration with the company involved in the implementation study. The tests also concluded that utilizing a sample time $T_{\mathrm{s}} < 15$

Table 1
Controller implementation parameters and setpoints.

(a) System constraints					
Parameter	$P_{\text{grid,max}}$	$P_{\text{evs,clip}}$	$P_{\text{evs,max}}$	$P_{\text{pv,max}}$	$N_{\text{connected,max}}$
Unit	kW	kW	kW	kW	–
Value	1000	88.32	1000	940	174

(b) Controller parameters							
Parameter	T_s	M_{days}	$J_{\max}$	β_y	β_{T1}	β_{T2}	β_s
Unit	min	days	–	–	–	–	–
Value	15	2	$1e14$	1	1	$1e{-}6$	$1e5$

(c) Vehicle charging setpoint and parameters						
Parameter	τ_1	τ_2	η	$E_{\text{ev,min}}$	$E_{\text{ev,requested}}$	$P_{\text{ev,requested}}$
Unit	hh:mm	hh:mm	%	kWh	kWh	kW
Value	16:00	23:00	98.5	21	23.5	7

(d) Faulty vehicle forecast and energy target adjustment parameters					
Parameter	e_{max1}	e_{max1}	e_{max1}	e_{max1}	α
Unit	–	–	–	–	
Value	10	6	6	5	0.7

Table 2
Comparison 01-02-2023 to 13-02-2023.

Indicator	Unit	01-02-2023	13-02-2023
Number of vehicles	[–]	64	73
Energy per vehicle	[kWh]	24.8	22.8
Energy per vehicle CDR[a]	[kWh]	*23.1*	*21.1*
PV energy	[kWh]	1651	1651
Self sufficiency	[%]	47.8	88.2
Grid power peak	[kW]	324	85
Grid negative power peak	[kW]	240	63
Grid obtained energy	[kWh]	829	196
Grid supplied energy	[kWh]	891	180

[a] Values obtained from charge detail records.

minutes would result in inconsistent and dysfunctional behavior of the load balance controller. Hence, 15 minutes was selected. The minimal control threshold $P_{\text{evs,clip}}$ was set to a minimum of three-phase 32 A per rail for five rails instead of six. It was observed that the sixth rail was not utilized.

5.2. Single day evaluation

A single day evaluation was performed to check the uncontrolled and controlled behavior of the system before and after implementing the MPC controller. The controlled system results for 13-02-2023 (controlled day) are compared to the results for 01-02-2023 (uncontrolled day). Fig. 9(a) indicates that a similar number of vehicles were connected to the charging infrastructure throughout both days. On 01-02-2023, the charging behavior was independent of the PV power. To make a fair comparison, on this day the PV power is assumed to be equal to 13-02-2023, such that P_{pv}[01-02-2023 00:00 to 01-02-2023 23:55] := P_{pv}[13-02-2023 00:00 to 13-02-2023 23:55]. The power for both days is plotted over time in Figs. 9(b) and 9(c). A comparison of relevant measurements and corresponding indicators are listed in Table 2.

The measured charge power P_{evs} and the input u_2 are plotted over time in Fig. 10. Vehicle charge behavior cannot be influenced before 8:00 in the morning. Between 11:30 and 14:00, the charge power is lower than the input. This is due to the overestimation of $P_{\text{ev,requested}}$. u_2 could have been followed with a lower error if $P_{\text{ev,requested}}$ was estimated correctly. However, overestimating ensures that all vehicles charge unrestricted during the peak PV power hours. The side-effect of this approximation is that the energy objective may not be met every day.

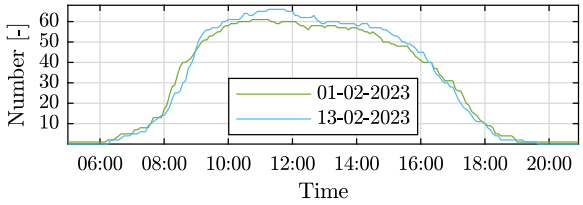

(a) Number of vehicles connected to the charging infrastructure over time.

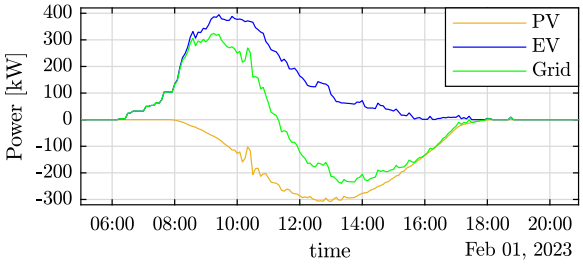

(b) Power over time uncontrolled day with artificial PV power.

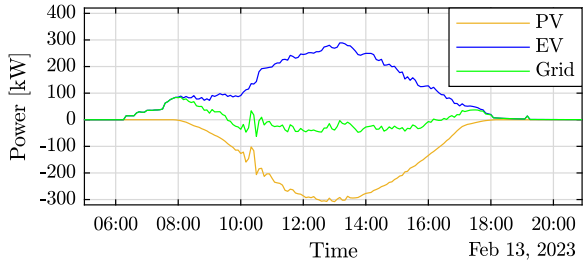

(c) Power over time controlled day.

Fig. 9. Comparison uncontrolled day 01-02-2023 to controlled day 13-02-2023.

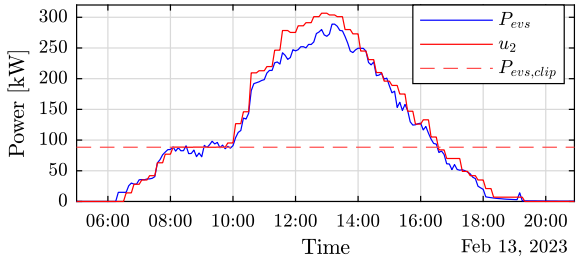

Fig. 10. Vehicle charge power and input over time 13-02-2023.

Fig. 11 depicts system behavior and its predicted trajectories at specific times throughout the day. Fig. 11(a) shows that the vehicle occupancy forecasts exhibit unrealistic fluctuations. These fluctuations may be reduced by implementing a forecast filter or by adding an extra feature to the forecasting XGBoost model. However, the effect on the controller performance is not visible. Fig. 11(b) indicates that the PV power ramped up later than initially predicted. The change in the optimal input-trajectory is depicted in Fig. 11(c). The high sample time makes it impossible for the controller to compensate for PV power noise over time. The charged energy over time is visible in Fig. 11(d), where the adjustment of the first energy objective is emphasized.

5.3. Three weeks evaluation

In this section, the controller behavior for a longer period is compared with the uncontrolled scenario. The controller was operational during weeks 6, 7, and 8 of 2023, but it was not during weeks

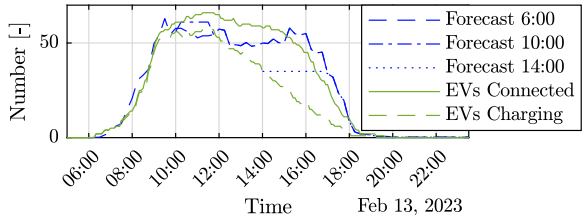

(a) Number of connected vehicles over time. Vehicle forecasts are adjusted for fully charged vehicles.

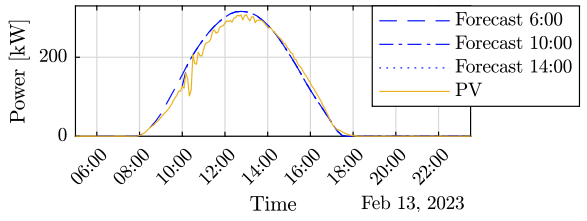

(b) PV Power.

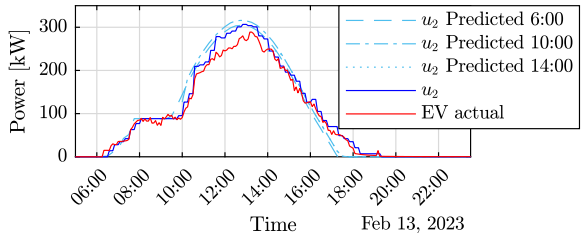

(c) Vehicle charge power.

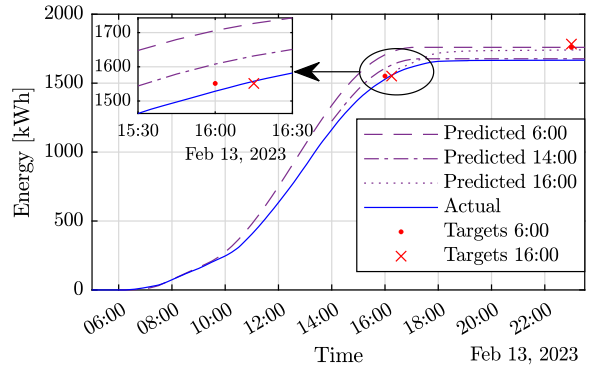

(d) Vehicle charge energy and adjusted objectives.

Fig. 11. MPC and external forecast over time. Only the first day in prediction horizon is depicted.

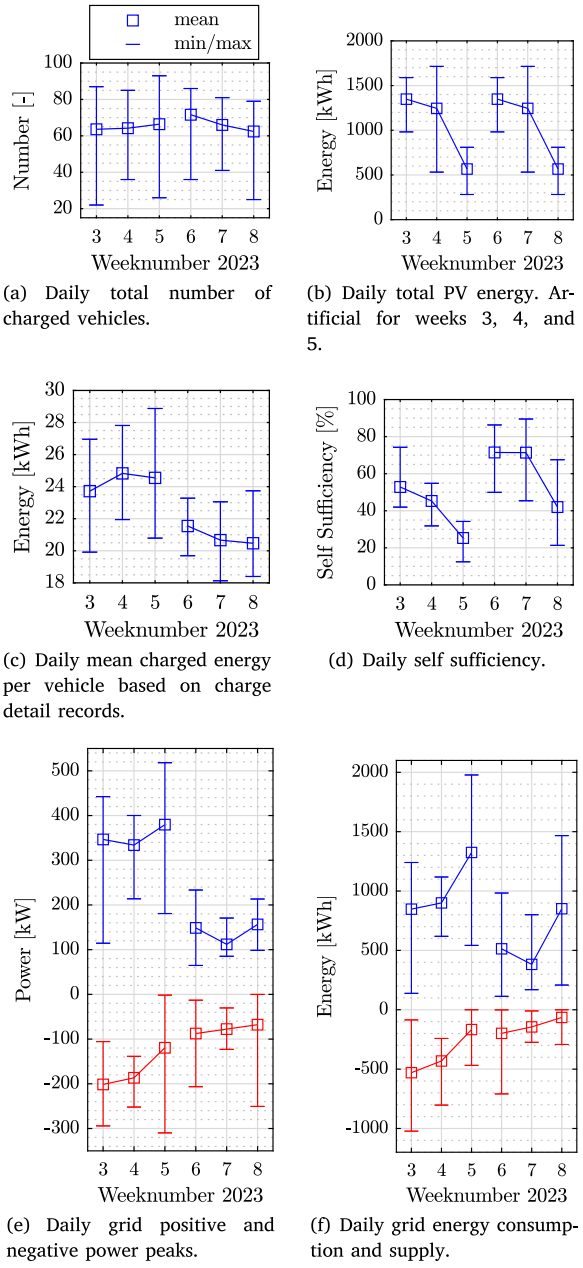

(a) Daily total number of charged vehicles.

(b) Daily total PV energy. Artificial for weeks 3, 4, and 5.

(c) Daily mean charged energy per vehicle based on charge detail records.

(d) Daily self sufficiency.

(e) Daily grid positive and negative power peaks.

(f) Daily grid energy consumption and supply.

Fig. 12. Based on Mondays to Fridays, weekly statistics of daily performance indicators. Three uncontrolled (3, 4, 5) and three controlled (6, 7, 8) weeks.

3, 4, and 5. A comparison between the two sets of three weeks is made. Again, to make a fair comparison, the PV power of the uncontrolled weeks is artificially set equal to the controlled weeks such that P_{pv}[16-01-2023 00:00to 29-01-2023 23:55] := P_{pv}[30-01-2023 00:00 to 26-02-2023 23:55]. Daily statistics for all workdays (Mo. – Fr.) are obtained. Per week, the minimum, maximum, and mean are plotted in Fig. 12. For example, Fig. 12(e) indicates that the lowest daily positive grid peak power for week 3 was 114 kW, while the average daily peak power over that week was 347 kW. Histograms depicting the total vehicle charge energy based on the charge detail records for the three uncontrolled and controlled weeks are depicted in Fig. 13.

The day-to-day percent peak-power differences for the 15 controlled and uncontrolled days are calculated. During the controlled days, the positive peak powers are reduced by an average of 59%, while the negative peak powers are reduced by an average of 47%. On average, three more vehicles were charged per day during the controlled weeks. Self-sufficiency increased from 41% to 62%. It has to be noted that according to the charge detail records, the average energy per session reduced from 24.4 kWh to 20.1 kWh. Also, a few vehicles had to re-initiate a charging session, splitting the total charge energy over two sessions instead of one.

5.4. Implementation issues

In the three weeks of operating the controller, 1226 charging sessions took place with 160 different vehicles. Two of those vehicles could not charge correctly after the MPC implementation. The vehicles promptly terminated their charging session when the charge point paused the session. Also, minimal current-amplitude values lower than 32 A per rail were tested. The load balance controller in those scenarios could not distribute the current evenly and fluctuated in current per vehicle chargers with an apparently too high frequency. This resulted

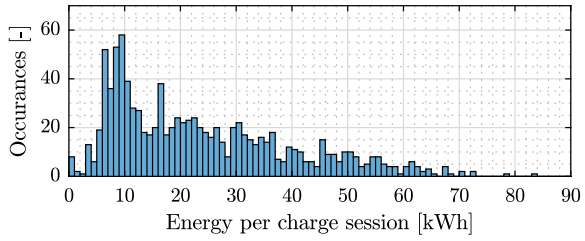

(a) Energy distribution uncontrolled 3 weeks.

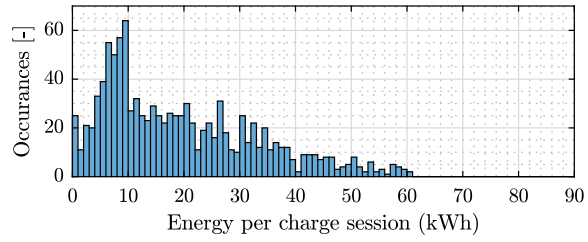

(b) Energy distribution controlled 3 weeks.

Fig. 13. Charge detail records.

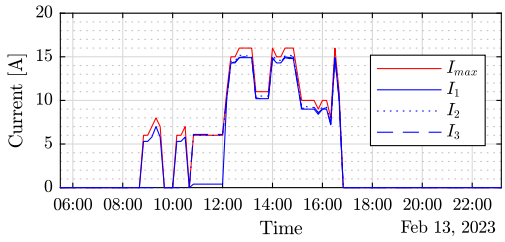

Fig. 14. Actual and available charging current for a single vehicle charging session.

in vehicles terminating the charging session. Load balance controller results are provided as supplementary material.

5.5. Limitations

One limiting factor of the designed controller is the assumption regarding charge power limits. The maximum vehicle charge power is overestimated around noon, which is visible in Fig. 10. Meanwhile, the maximum vehicle charge power is underestimated later in the afternoon, which becomes apparent when analyzing the charge data of the individual vehicles. A session where this is visible around 15:30 is depicted in Fig. 14. The result is sub-optimal because power is delivered back to the grid around 15:30, as indicated in Fig. 9(c). More individual charging session behavior results are provided as supplementary material. The decision space of u_2, visible in Fig. 4, depends on the assumptions of P_{ev}. For $k = k_0$, $\hat{N}_{\text{evs,charging}}$ is a measurement and P_{ev} is a parameter. If the controller can access real-time individual charge pole data, it could infer if a vehicle charges with maximal available power. This information can improve the estimation of the limits $\tilde{u}_{2\text{min}}$ and $\tilde{u}_{2\text{max}}$. Improving the estimated limits will improve the controller performance.

The second limiting factor of the controller is visible in Fig. 9(c), where the minimal charge power $P_{\text{evs,clip}}$ enforces grid power consumption around 8:00 and 17:00. The choice of $P_{\text{evs,clip}}$ is based on a minimum current per rail of 32 A, a constraint set by the load balance controller. A vehicle needs at least a current of 6 A per phase to initiate a charging session. The charger can pause the session directly after initiation. The reason for the minimum of 32 A seems arbitrary, and creating a load balance controller that pauses all vehicle charging sessions simultaneously should be possible.

The controller is implemented to charge infrastructure that is part of an office building complex. The power demand of the charging infrastructure is altered with no consideration given to the power consumption of the office buildings. The implementation can be extended by including additional forecasts of extra disturbances to (23a). The same objectives could be met while considering the actual grid load of the entire office complex.

Finally, regarding adaptability to different systems, the control solution can be implemented at locations with comparable charging behavior. The periodic charging behavior of vehicles at office locations allows for determining precise energy objective times. The controller is flexible in terms of system size and can be applied to larger-scale systems. The controller can likely be applied to smaller-scale systems if improvement is made in estimating the charge power limits. However, it may not be feasible to implement the control solution in places where a higher variance in arrival and departure times of vehicles exists, such as in public charging stations or very small EV occupation. The inability to control individual charging sessions would be a limitation in such cases.

6. Conclusion

This study successfully solved and implemented an optimal control problem of minimizing the local power supply and demand imbalance in a grid-connected microgrid through vehicle charge control. A batch-type model predictive controller is developed and implemented to minimize the grid power amplitude and maximize vehicle charging using PV power. Considering the daily energy needs for charging vehicles as a batch is an essential aspect. The controller is effectively integrated into an existing SCADA system by incorporating external forecasting systems and setting reference signals for lower-level controllers. The attainment of the control objectives demonstrated the overall effectiveness of the system implementation. The study is deemed successful as the controller was kept operational after the three-week test period. Moreover, an average daily grid peak power reduction of 59% was achieved.

Controlling the system on an aggregated level enables the implementation of the controller into existing systems. Performance may be improved by enabling communication with individual vehicle chargers. Regarding the specific use case, a recommendation can be made to revise the internal workings of the load balance controller, as it seems that the operating constraints are set conservatively. The control solution performs adequately in an office environment, but it might not be suitable for charging infrastructure that exhibits a higher variance in arrival and departure times.

CRediT authorship contribution statement

B.A.L.M. Hermans: Writing – original draft, Visualization, Validation, Software, Methodology, Investigation, Conceptualization. **S. Walker:** Writing – review & editing, Writing – original draft, Supervision, Project administration, Methodology, Conceptualization. **J.H.A. Ludlage:** Writing – review & editing, Supervision, Conceptualization. **L. Özkan:** Writing – review & editing, Supervision, Conceptualization.

Declaration of competing interest

The authors declare that they have no known competing financial interests or personal relationships that could have appeared to influence the work reported in this paper.

Data availability

The data that has been used is confidential.

Acknowledgments

The first author would like to express his gratitude for Kevin de Bont, Joep van der Velden, Jan-Willem Dubbeldam and Team TCC from Kropman BV. Furthermore, the research could not have taken place without the generous cooperation of Jos de Ruijter from the case study building, which allowed for extensive testing on their infrastructure.

Appendix A. Supplementary data

Supplementary material related to this article can be found online at https://doi.org/10.1016/j.apenergy.2024.123210.

References

[1] Liang X. Emerging power quality challenges due to integration of renewable energy sources. IEEE Trans Ind Appl 2017;53:855–66. http://dx.doi.org/10.1109/TIA.2016.2626253.

[2] Majzoobi A, Khodaei A. Application of microgrids in supporting distribution grid flexibility. IEEE Trans Power Syst 2017;32:3660–9. http://dx.doi.org/10.1109/TPWRS.2016.2635024.

[3] Solar power in the netherlands: is that a duck? 2024, URL https://www.matteodefelice.name/post/netherlands-is-that-a-duck/.

[4] ACM. ACM investeringsplannen netbeheerders tonen tekort aan transportcapaciteit door groeiende vraag. URL https://www.acm.nl/nl/publicaties/acm-investeringsplannen-netbeheerders-tonen-tekort-aan-transportcapaciteit-door-groeiende-vraag.

[5] Wilson, Alex Benjamin. Revision of the energy performance of buildings directive: Fit for 55 package. 2023, Briefing, Briefing document on the ongoing legislative processes within the European Union.

[6] Karthikeyan N, Pokhrel BR, Pillai JR, Bak-Jensen B. Utilization of battery storage for flexible power management in active distribution networks. In: IEEE power & energy society general meeting. 2018, p. 1–5.

[7] Riffonneau Y, Bacha S, Barruel F, Ploix S. Optimal power flow management for grid connected PV systems with batteries. IEEE Trans Sustain Energy 2011;2:309–20. http://dx.doi.org/10.1109/TSTE.2011.2114901.

[8] Raoufat ME, Asghari B, Sharma R. Model predictive BESS control for demand charge management and PV-utilization improvement. In: 2018 IEEE power & energy society innovative smart grid technologies conference. ISGT, 2018, p. 1–5. http://dx.doi.org/10.1109/ISGT.2018.8403403.

[9] Rassaei F, Soh WS, Chua KC. Demand response for residential electric vehicles with random usage patterns in smart grids. IEEE Trans Sustain Energy 2015;6:1367–76. http://dx.doi.org/10.1109/TSTE.2015.2438037.

[10] Galus MD, Wietor F, Andersson G. Incorporating valley filling and peak shaving in a utility function based management of an electric vehicle aggregator. In: 2012 3rd IEEE PES innovative smart grid technologies europe (ISGT europe). 2012, p. 1–8. http://dx.doi.org/10.1109/ISGTEurope.2012.6465894.

[11] Chen X, Ding Q, Qian G, Chen X, Huang C, Meng J. Optimal scheduling strategy with multi-time scales for PV-storage based charging station. In: 2020 IEEE sustainable power and energy conference. ISPEC, 2020, p. 2249–55. http://dx.doi.org/10.1109/iSPEC50848.2020.9351227.

[12] Zheng Y, Song Y, Hill DJ, Meng K. Online distributed MPC-based optimal scheduling for EV charging stations in distribution systems. IEEE Trans Ind Inf 2019;15(2):638–49. http://dx.doi.org/10.1109/TII.2018.2812755.

[13] Diaz C, Ruiz F, Patino D. Smart charge of an electric vehicles station: A model predictive control approach. In: 2018 IEEE conference on control technology and applications. CCTA, 2018, p. 54–9. http://dx.doi.org/10.1109/CCTA.2018.8511498.

[14] Bracco S, Delfino F, Pampararo F, Robba M, Rossi M. A dynamic optimization-based architecture for polygeneration microgrids with tri-generation, renewables, storage systems and electrical vehicles. Energy Convers Manage 2015;96:511–20. http://dx.doi.org/10.1016/j.enconman.2015.03.013.

[15] InsiteSuite URL https://insitesuite.nl/.

[16] Somers W. Forecasting individual and aggregated electric vehicle charging loads at offices with machine learning. 2022.

[17] Franklin GF, Powell JD, Workman ML. Digital control of dynamic systems. third ed.. Addison-Wesley; 1998, p. 400–19.

[18] Solar forecast for PV. URL https://solargis.com/products/solar-power-forecast/overview.

[19] Andersen MS, Dahl J, Vandenberghe L. CVXOPT: A python package for convex optimization, version 1.3.0. 2022, URL https://cvxopt.org/.

[20] Somers W. Effects of data-driven forecasting models on controlling energy management systems. 2023, URL https://brains4buildings.org/wp-content/uploads/2023/06/20230413-TUeMaster_Thesis_Somers_Ward.pdf.

[21] Somers W, Khan W, de Bont K, Zeiler W. Individual EV load profiling and smart charging to flatten total electrical demand. In: CLIMA 2022 conference. 2022, http://dx.doi.org/10.34641/clima.2022.164, URL https://proceedings.open.tudelft.nl/clima2022/article/view/164.

[22] Khan W, Somers W, Walker S, de Bont K, Van der Velden J, Zeiler W. Comparison of electric vehicle load forecasting across different spatial levels with incorporated uncertainty estimation. Energy 2023;283:129213. http://dx.doi.org/10.1016/j.energy.2023.129213, URL https://www.sciencedirect.com/science/article/pii/S0360544223026075.

[23] Bernard S, Heutte L, Adam S. Towards a better understanding of random forests through the study of strength and correlation. In: Huang D-S, Jo K-H, Lee H-H, Kang H-J, Bevilacqua V, editors. Emerging intelligent computing technology and applications. with aspects of artificial intelligence. Berlin, Heidelberg: Springer Berlin Heidelberg; 2009, p. 536–45.

[24] Chen T, Guestrin C. XGBoost: A scalable tree boosting system. In: Proceedings of the 22nd ACM SIGKDD international conference on knowledge discovery and data mining. KDD '16, New York, NY, USA: ACM; 2016, p. 785–94. http://dx.doi.org/10.1145/2939672.2939785, URL http://doi.acm.org/10.1145/2939672.2939785.